Progress In Electromagnetics Research C, Vol. 100, 1–16, 2020

An Integrated Shark-Fin Reconfigurable Antenna for V2X Communications

Dimitris K. Rongas[1, *], Anastasios S. Paraskevopoulos[2], Leonidas D. Marantis[2], and Athanasios G. Kanatas[2]

Abstract—This paper focuses on the design, development, and integration of a V2X shark-fin antenna. A novel planar Electronically Switched Parasitic Array Radiator (ESPAR) antenna, operating at 5.9 GHz, is proposed. The antenna exhibits pattern reconfigurability, i.e., one quasi-omni and two directive beams, low cost, reduced complexity, and small dimensions. Therefore, it is considered as an ideal candidate for integrating inside a shark-fin casing. The ESPAR antenna prototype is fabricated and tested in three different measurement scenarios: (a) free-space, (b) inside shark-fin, and (c) shark-fin with ground plane. A good correlation between simulated and experimental results has been obtained. The proposed antenna involves a reconfigurable impedance matching network that is integrated in the antenna design, and thus, it demonstrates a satisfactory impedance matching for all antenna states. A considerable gain enhancement (3–4 dB) is also recorded between the omnidirectional and two directive patterns.

1. INTRODUCTION

Vehicle-to-Everything (V2X) communications along with Intelligent Transportation Systems (ITS) have made an important contribution to the area of vehicular transportations and automotive industry [1]. As a result, several transportation prospects, such as traffic efficiency, driver's safety, reduction of car collisions, autonomous driving, and green transportation (offering reduction of fuel consumption and carbon emissions) have been improved during the last decade, aiming at an efficient, low cost, and environment-friendly transportation for billions of users [2]. The increase of system capacity and the reliability of Vehicle-to-Vehicle (V2V) communication links are the two main requirements associated with the performance of modern ITS systems and have to be considered during the antenna design process.

However, in order to resolve these two technical issues, there are five basic challenges that are encountered in vehicular communications and have to be thoroughly examined [3]: (a) Highly dynamic environment with severe multipath effects, (b) Intense scattering caused by the vehicle's cabin and numerous other metal surfaces distributed in a close distance, (c) Strong interference due to low power/wide band signals, (d) Full azimuth coverage for broad-casting, (e) Low cost, reduced complexity, and compact size antenna solutions that are easily integrated on the roof of the vehicle.

Numerous MIMO techniques, i.e., spatial multiplexing, diversity, and beam forming, have been proposed in order to resolve the aforementioned challenges and achieve a satisfying performance of V2X links. Nevertheless, the majority of the antenna models that have been employed in the recent ITS systems consist of typical designs with a single radiating element, i.e., wire/printed monopole or PIFA, usually located in a shark-fin casing on the vehicle's roof [4, 5]. These cases cannot support any

Received 20 November 2019, Accepted 31 January 2020, Scheduled 18 February 2020
* Corresponding author: Dimitris K. Rongas (drongas@mobile.ntua.gr).
[1] School of Electrical and Computer Engineering, National Technical University of Athens, Greece. [2] Department of Digital Systems, School of ICT, University of Piraeus, Greece.

digital techniques since they provide a fixed radiation pattern. There are certain examples of antenna arrays (or multiple antenna systems) that have been designed and integrated on vehicles. However, they exhibit several disadvantages such as large dimensions, high complexity, and high cost [6–8]. The same disadvantages are also encountered in a few proposed MIMO antenna systems that are embedded in a shark-fin structure [9–11].

A reconfigurable antenna able to achieve multiple radiation patterns is an ideal candidate to substitute a multiple antenna system and overcome the size, complexity, and cost constraints imposed by the automotive industry. Pattern reconfigurability can be an important asset in V2X communications since it offers the ability to employ various diversity techniques, e.g., beam selection or hybrid beam/antenna selection, in order to enhance ITS system performance in terms of capacity and reliability [12, 13]. Although there are a few reported V2V reconfigurable antenna designs [14–16], none of them focuses on the integration of the antenna on the vehicle and especially in a shark-fin casing.

The ESPAR antenna is a special type of parasitic antenna array that involves a single active element, therefore, only one RF chain. However, it maintains numerous characteristics of a MIMO system, such as beam forming and spatial multiplexing capabilities [17–19]. The second basic characteristic of the ESPAR antenna is the fact that the rest of the radiators are passive parasitic elements, distributed around the active element in several arrangements and in small distances ($\lambda/4$–$\lambda/16$). These two features of ESPAR antennas lead to various advantages such as significantly reduced complexity, low fabrication cost, and compact size [20, 21]. As a result, ESPARs can be considered as ideal candidates for vehicular integration, where in most cases, the available space is restricted, e.g., inside a shark-fin casing. There are numerous publications in the literature that investigate ESPAR antennas employing various types of radiating elements, i.e., wire monopole antennas [19, 22, 23], printed dipoles [24, 25], slots [26], printed patches [27], and printed PIFAs [28, 29]. However, only in [30] an ESPAR of printed monopoles, operating above 5 GHz, is fabricated and experimentally tested, focusing though on channel performance. To the best of our knowledge, our research group was the first that proposed a printed monopole ESPAR antenna, designed and experimentally verified for a frequency close to 6 GHz (5.9 GHz) for V2X communications [13]. In the present paper, these antenna designs [13, 31, 32] are considerably optimized by offering, for the first time, two significant novelty points among others: (a) integration of a switched impedance matching network in the ESPAR design and (b) integration of the ESPAR in a shark-fin structure.

The remainder of the paper exhibits the following outline. Section 2 describes the antenna configuration and EM modelling setup. In Section 3, the fabrication process is briefly described, and the performance of the novel ESPAR antenna is investigated for three different scenarios: (a) in free space, (b) inside the shark-fin casing, and (c) inside the shark-fin casing on top of a ground plane. The simulated and measured results (S_{11} and radiation patterns) of the proposed antenna are demonstrated. Finally, Section 4 provides the final conclusions from our investigations.

2. ANTENNA DESIGN AND EM MODELLING

2.1. Antenna Design

The proposed antenna is designed in a planar configuration to fit inside the shark-fin casing that appears on most modern vehicle roofs. The radiating elements are printed on a Rogers R0-4725JXR dielectric substrate ($\epsilon_r = 2.55$, $\tan\delta = 0.0026$, $h = 0.78\,\text{mm}$). The occupied area of the resulting antenna is $37 \times 32\,\text{mm}$. Fig. 1 illustrates the top and bottom layers of the ESPAR antenna together with the final antenna dimensions, which are also listed in Table 1.

The antenna operation is based on direct and indirect radiation of three printed monopoles that are designed in close proximity ($\lambda/5$) to each other. The central active $\lambda/4$ monopole is connected through a microstrip quarter-wavelength ($\lambda/4$) transformer to the $50\,\Omega$ feed line, as the transformer matches the $50\,\Omega$ impedance to the $37\,\Omega$ theoretical input impedance. The close distance between the active and parasitic elements produces strong mutual coupling and induces currents on the parasitics, enabling the formation of directive beams. The side parasitic monopoles are connected to ground through platted vias (through holes). Moreover, two PIN diodes operate as ON/OFF electronic switches and connect the two parasitic elements to the grounded metal pads. PIN diodes are employed since they demonstrate

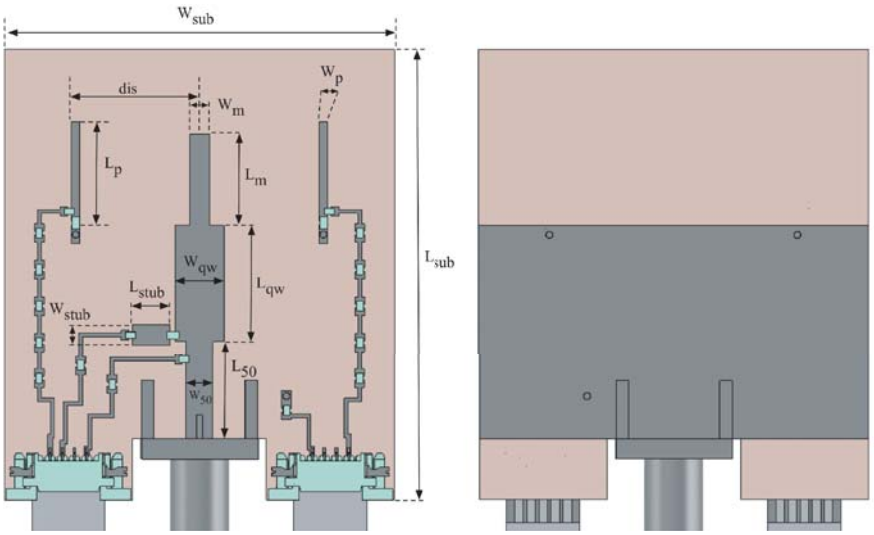

Figure 1. (a) Top view with the basic design parameters and (b) bottom view of the printed ESPAR antenna.

Table 1. Optimized antenna dimensions in millimeters.

Dimension	Value	Dimension	Value
L_m	7.5	L_{qw}	9.55
W_m	1.63	W_{qw}	4
L_p	8.1	L_{stub}	3.1
W_p	0.7	W_{stub}	1.7
L_{sub}	37	L_{50}	8
W_{sub}	32	W_{50}	2.2
dis	10.21	h	0.78

faster switching (typically < 100 ns) and considerably smaller packaging than RF mechanical switches. By switching ON and OFF each of the parasitic elements, a total of 3 different radiation patterns can be produced: one omnidirectional pattern for broadcasting and two directive patterns in the forward (F) and backward (B) vehicle directions. Specifically, when the PIN diode is ON, the printed monopole is connected to the metal pad and thus, to the ground plane at the back side of the panel. As a result, an L-shaped metal strip is created reflecting the radiation and constructing a directive beam towards the opposite side.

A main disadvantage of the ESPAR antennas, as it has been reported in our previous works [13, 31, 32], is the significant deviations in the reflection coefficient (S_{11}) that occur among the different antenna states, due to the different current distributions on the parasitic elements and its effect on the antenna's input impedance. For this reason, a reconfigurable stub matching approach is employed involving a single-stub shunt tuning circuit in order to correct the deviations. Specifically, a switched impedance matching network is incorporated in the microstrip design to tune the antenna at 5.9 GHz when being needed. The reconfigurable impedance matching network is implemented by adding an open microstrip stub, connected in parallel to the microstrip transmission line through a PIN diode.

Regarding the selection of the PIN diodes employed in the antenna design, the Skyworks SMP-1320 diode model is preferred due to the low values of 0.9Ω series resistance and 0.3 pF capacitance that are observed in the ON and the OFF states, respectively. These properties along with the small

package profile (040LF with 1×0.5 mm) guarantee a negligible disturbance in antenna gain. SMP-1320 also exhibits a high switching speed (0.4–40 ns), which benefits the reconfigurability of the ESPAR and allows the antenna to support pattern diversity techniques. A DC biasing network is also included to provide the necessary voltage (0.85 V) to the PIN diode terminals. A series of 18 nH inductors (Coilcraft 0302CS-18NXJLU with 6.03 GHz SRF) are also employed to block the AC current flow to the DC bias network and preserve this way the radiation pattern of the antenna undisturbed. The DC lines are broken down in smaller pieces by inserting RF choke inductors in order to avoid any unwanted radiation from the DC bias lines, due to mutual coupling effects. Finally, a very thin antenna profile, specified by the thickness of the substrate, is achieved by using flat FFC DC connectors instead of protruding DC pins, allowing the integration inside the shark-fin structure and the routing of all the cables in one direction.

2.2. EM Modelling

The antenna is modelled using the CST 3D electromagnetic suite [33]. The 3D simulation model of the antenna (as shown in Fig. 1) is composed of the following four parts: a printed circuit board (PCB), lumped elements of the PIN diodes and the inductors along with the surface mount device (SMD) packaging, DC biasing connectors and cables, and an RF connector. Due to the omnidirectional nature of the printed monopole antenna, the length of the cables is found to affect the accuracy of the simulation result. Therefore, the bottom (Ymin) boundary in the computational space is set to perfectly matched layer (PML) or "Open" to emulate an "infinite" cable length.

Another important aspect of the antenna simulation accuracy is the modelling of SMD electronic components as lumped elements. In most literature of reconfigurable-ESPAR antennas, the two PIN diode states (ON and OFF) are modelled with two different RLC equivalent circuits, fixed for the frequency of operation. In this work, the complete 2×2 measured diode S-parameter matrix, provided by the manufacturer (S2P file for 0.85 V/10 mA at ON state and 0 V at OFF state) is employed for each diode state, accurately representing the PIN diode behavior versus frequency. As for the modelling of the RF chokes, the SPICE model of the inductor is used for the simulation of the lumped element.

3. ANTENNA FABRICATION AND PERFORMANCE

3.1. Free Space Antenna Performance

The antenna is fabricated using the standard chemical etching technique, and all the electronic SMD components (PIN diodes, inductors, SMA connector, DC FFC connectors) are placed and soldered by hand. The fabricated prototype of the proposed reconfigurable antenna is shown in Fig. 2. The photograph clearly depicts the compact dimensions of the antenna and highlights the ability of achieving pattern reconfigurability in such a small antenna structure.

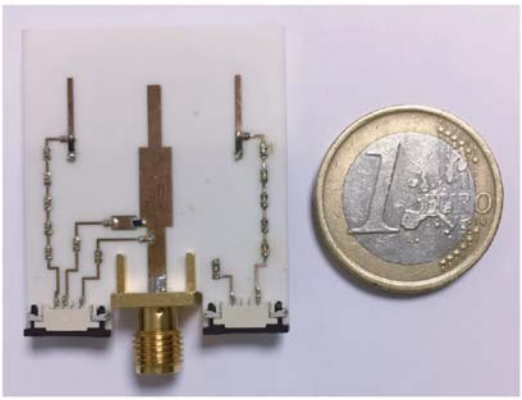

Figure 2. Fabricated printed monopole (ESPAR) antenna.

The reflection coefficient of the antenna is measured using the Vector Network Analyzer (Keysight N5221A). The simulated and measured S_{11} reflection coefficients of the antenna by sequentially switching ON/OFF all the available PIN diodes are shown in Fig. 3 and Fig. 4, respectively (OFF-OFF stub-off, OFF-OFF stub-on, ON-OFF, OFF-ON). It is seen that a reflection level better than -15 dB is maintained for all the antenna operating states, and a close agreement between the simulated and measured results is achieved. This demonstrates the importance of accurate modelling of all the electronic components along with the modelling of the DC and RF connectors. Figs. 3 and 4 also exhibit an impedance bandwidth (-10 dB BW) of 400 MHz (above 7%) for all antenna states. Moreover, the functionality of the impedance matching network can be easily observed. When it is switched OFF, the S_{11} is at 6.1 GHz while in the ON state the resonance is tuned to the desired frequency.

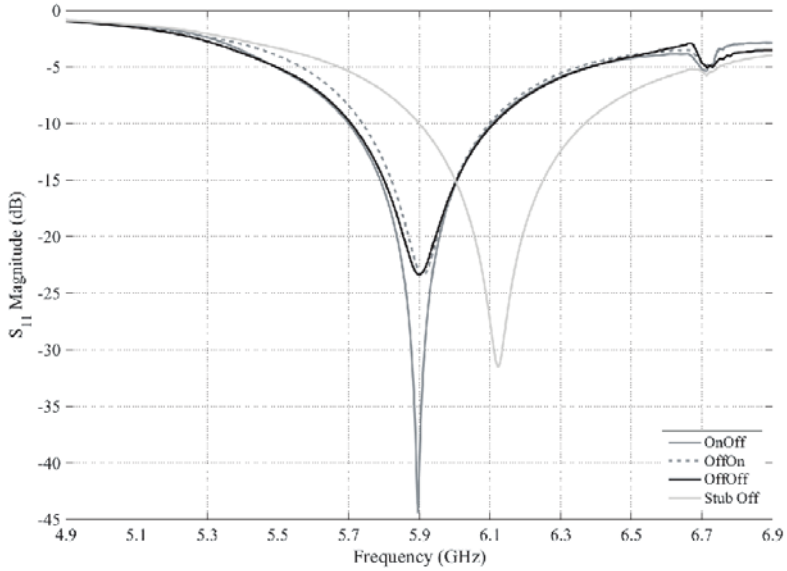

Figure 3. Simulated reflection coefficient (S_{11}) of the ESPAR antenna for all the operating states in free space.

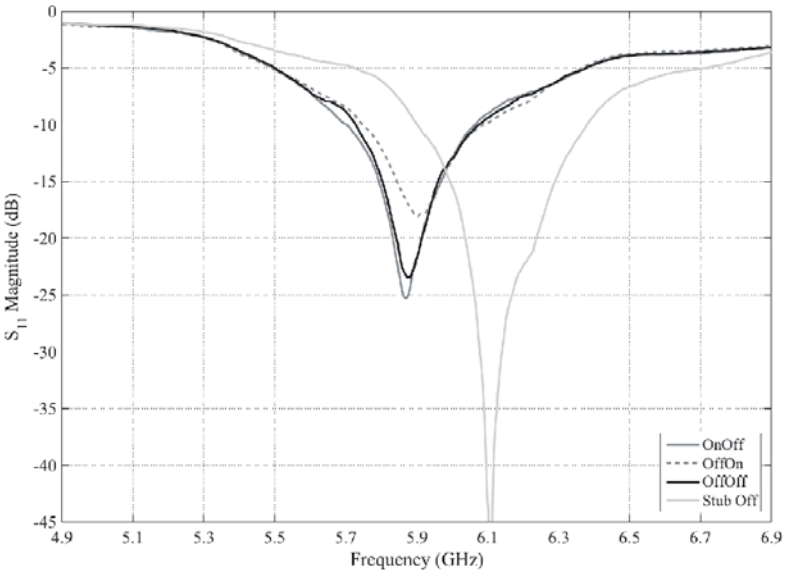

Figure 4. Measured reflection coefficient (S_{11}) of the ESPAR antenna for all the operating states in free space.

The measurement campaign took place in a shielded far-field anechoic chamber of IMST GmbH [34]. The system is based on a distributed vector network analyzer concept and is connected to a roll-over-azimuth scanning positioner enabling the radiation pattern measurement in the two principal planes. The gain-transfer method is used, by employing a Standard Gain Horn (14240 model by FMI, bandwidth of 5.38–8.18 GHz), in order to extract the absolute antenna gain. In Fig. 5, three different measurement setups of the antenna under test (AUT) are presented. Specifically, in Fig. 5(a) the antenna is in free space operation. In Fig. 5(b), it is mounted inside the shark-fin casing, and in Fig. 5(c), the shark-fin antenna is mounted on a 50×50 cm ground plane.

A schematic diagram is presented in Fig. 6 to contribute to a better understanding of the plotted planes. The H-plane is considered when scanning in φ with $\theta = 90°$, while the E-plane is considered

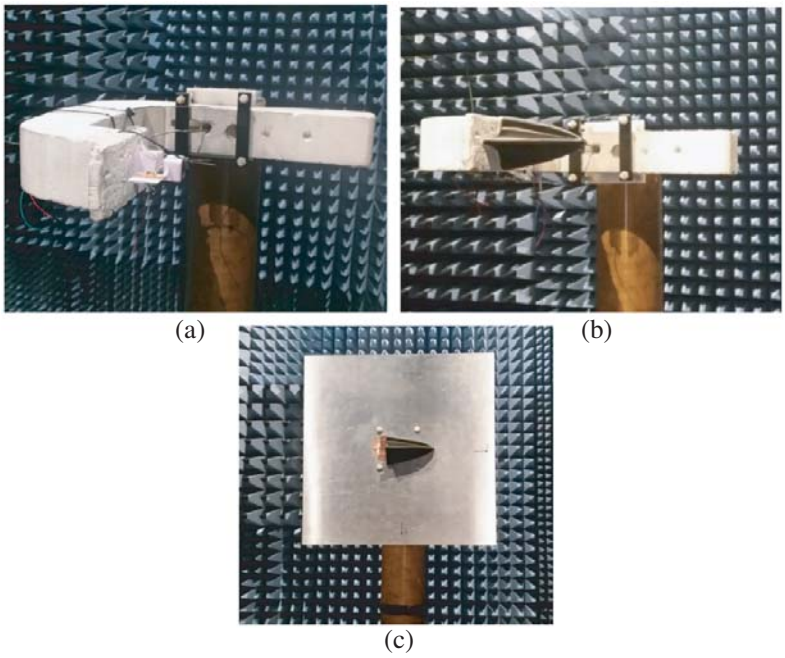

Figure 5. Measurement setup of the AUT inside the anechoic chamber: (a) antenna in free space, (b) antenna inside the shark-fin casing and (c) antenna inside the shark-fin casing on top of a 50×50 cm ground plane.

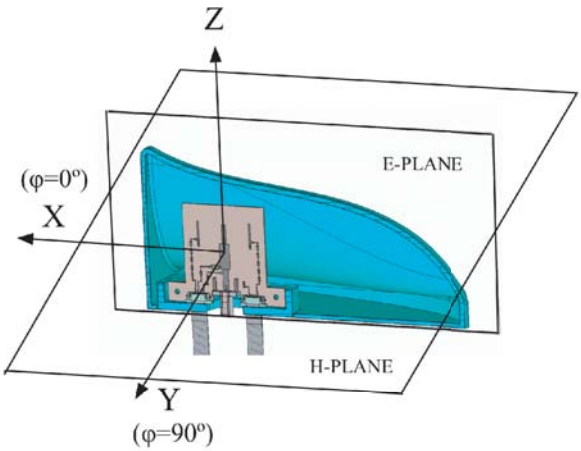

Figure 6. Schematic diagram of the antenna measurement coordinate system, together with the two (E-plane and H-plane) principal planes.

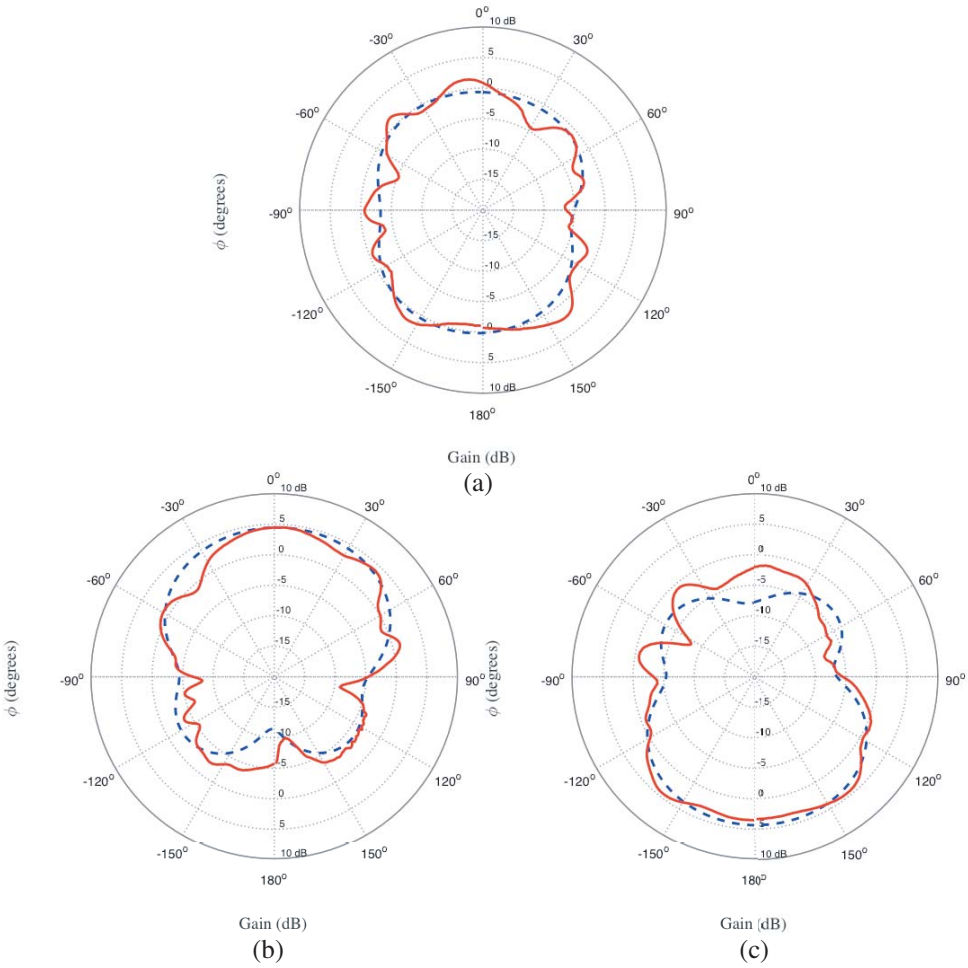

Figure 7. Measured (solid line) and simulated (dashed line) radiation patterns of the realised gain in the H-plane ($\varphi = 180°$) for the (a) OFF-OFF state, (b) OFF-ON state and (c) ON-OFF state of the ESPAR antenna in free space.

when scanning in θ with $\phi = 180°$. The resulting radiation patterns are plotted in terms of the realised gain of the antenna in free space for the H- and E-planes in Fig. 7 and Fig. 8, respectively. Overall, a close agreement between the measurement and simulation results is observed.

It is generally observed that the radiation patterns at the H-plane appear smooth while some minor ripples can be found in the E-plane (Fig. 8). These ripples can be attributed to the procedure followed during the measurement acquisition. The scanning at the E-plane is done by rotating the antenna via the azimuth axis causing an inevitable interaction with the positioner, while the scanning at the H-plane is done by rotating the roll axis, and therefore, there is no effect from the positioner.

The OFF-OFF state (Fig. 7(a)) presents a non-perfectly (quasi) omnidirectional radiation pattern, with gain levels reduced by few dB at $\varphi = 90°$ and $\varphi = -90°$ due to the printed ground plane topology, while at $\varphi = 0°$ and $\varphi = 180°$, the level of antenna gain is at a 0 dB absolute value. This behavior can be attributed to the planar structure of the antenna along the x axis and the fact that the ground plane is accommodated on the same plane as the printed monopoles and not located on the perpendicular azimuth plane.

When the required DC voltage is applied at either of the PIN diodes located between the parasitic elements and metal pads (OFF-ON or ON-OFF state), the parasitic element is connected to the ground plane, forming a reflector. As a result, the radiation pattern becomes directional, with the maximum gain appearing at the opposite side of the grounded parasitic element. As far as the OFF-ON state is

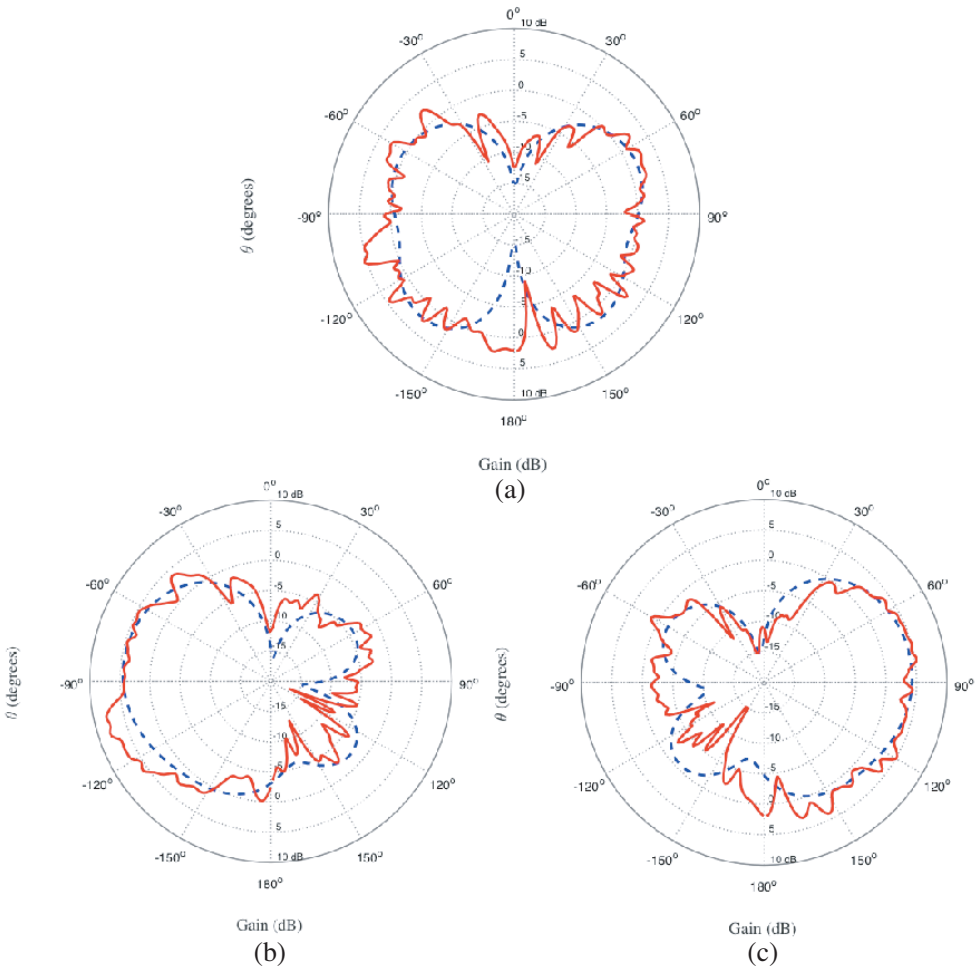

Figure 8. Measured (solid line) and simulated (dashed line) radiation patterns of the realised gain in the E-plane ($\theta = 90°$) for the (a) OFF-OFF state, (b) OFF-ON state and (c) ON-OFF state of the ESPAR antenna in free space.

concerned (Fig. 7(b)), the gain at $\varphi = 0°$ is 4.5 dB while at OFF-OFF state it is 0.85 dB, offering a gain improvement of 3.65 dB. As for the ON-OFF (Fig. 7(c)), the gain at $\varphi = 180°$ is 3.5 dB instead of -0.74 dB at the OFF-OFF state, offering a gain improvement of 4.24 dB. In Fig. 8, the radiation pattern in the E-plane is presented. The antenna pattern exhibits a symmetrical behavior, demonstrating equal gain at the two side edges of the ESPAR structure (at $\theta = \pm 90°$). Moreover, a reduced upward pattern tilt is observed. This is an important requirement for antennas intended for V2V communications. A maximum realised gain of 5.4 dB is obtained at $\theta = 82°$ (8° tilted upwards) for the ON-OFF state (Fig. 8(c)). The same behavior is applied at the OFF-ON state.

3.2. Shark-Fin Integrated Antenna Performance

Figure 9 illustrates the second measurement scenario setup, where the ESPAR antenna is integrated in a specially designed shark-fin casing ($L = 12.5\,\text{cm} \times W = 7.5\,\text{cm} \times H = 6\,\text{cm}$) made of polycarbonate ABS material ($\epsilon_r = 3.3$, thickness of 1.5 mm) using a Fused Deposition Modelling 3D printer. The shark-fin casing is the most common structure used on the roofs of modern cars in order to accommodate various automotive antennas and at the same time preserve the aerodynamic shape of the vehicle.

A 100 MHz frequency detuning to 5.8 GHz appears in both the simulated (Fig. 10) and measured (Fig. 11) return loss results for the three operating states. This is due to the interaction of the antenna with the shark-fin dielectric, which is in the near-field region of the antenna. To cope with the destructive

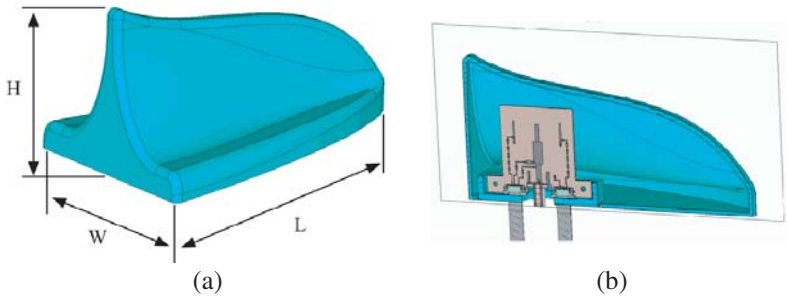

Figure 9. (a) Shark-fin 3D model and (b) cut-plane with the embedded antenna.

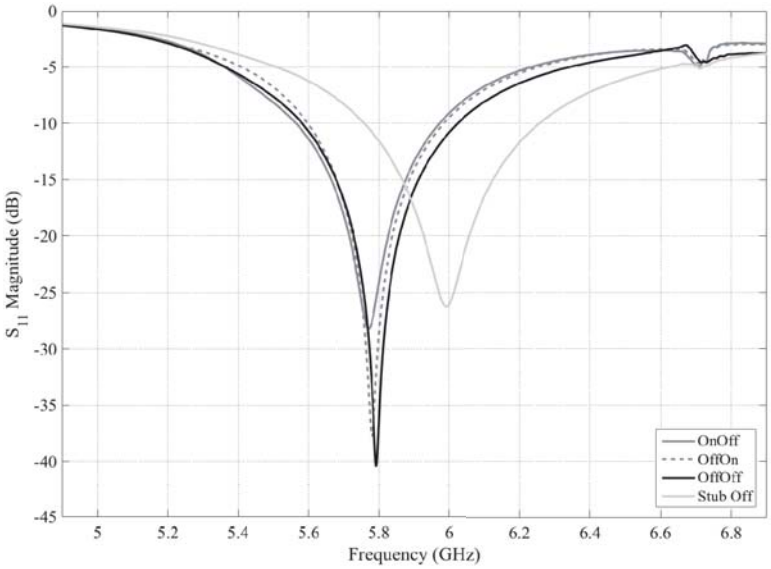

Figure 10. Simulated reflection coefficient (S_{11}) of the printed ESPAR antenna mounted inside the shark-fin.

detuning effect, some dimensions (Table 1) of the integrated antenna have been adjusted to operate at 5.9 GHz (L_m = 7.2 mm and L_p = 7.8 mm). The S_{11} results for the redesigned antenna version are presented in Figs. 12 and 13. The simulated S_{11} reflection coefficient remains below −30 dB while the measured value is below −20 dB for all the antenna operating states. It can be observed that the deviations between simulated and measured results are slightly greater than the previous measurement scenarios. The deposition method and the thermal process of the 3D printer can cause slight alterations on the relative permittivity of the final material used for the shark-fin structure.

In the case of the shark-fin integrated antenna, the radiation pattern, plotted in Fig. 14 and Fig. 15, exhibits a comparable performance with the free space case. The gain improvement between the directive and omnidirectional states remains unaffected from the shark-fin integration. The maximum realised gain at the OFF-ON state is 4.4 dB (it was 4.5 dB at the free space), showing no performance deterioration. At the ON-OFF state the maximum gain is 5.7 dB while it was 3.5 dB in free space. The increase in directivity is due to the elongated shape of the shark-fin casing in the forward direction. Hence, a gain imbalance of 2.3 dB between OFF-ON and ON-OFF states is evident due to the non-symmetrical shape of the shark-fin. This specific shape causes a different dielectric loading at $\varphi = 0°$ and $\varphi = 180°$ directions. A possible solution would be to design the antenna deliberately with an opposite gain imbalance so that the different dielectric loadings cancel out when being integrated in the shark-fin, or choosing a symmetrical spherical/cylindrical shark-fin shape that might not be aerodynamically accepted. The ripples that are observed in Fig. 15 are again caused by the procedure followed during the measurement acquisition as in Fig. 8.

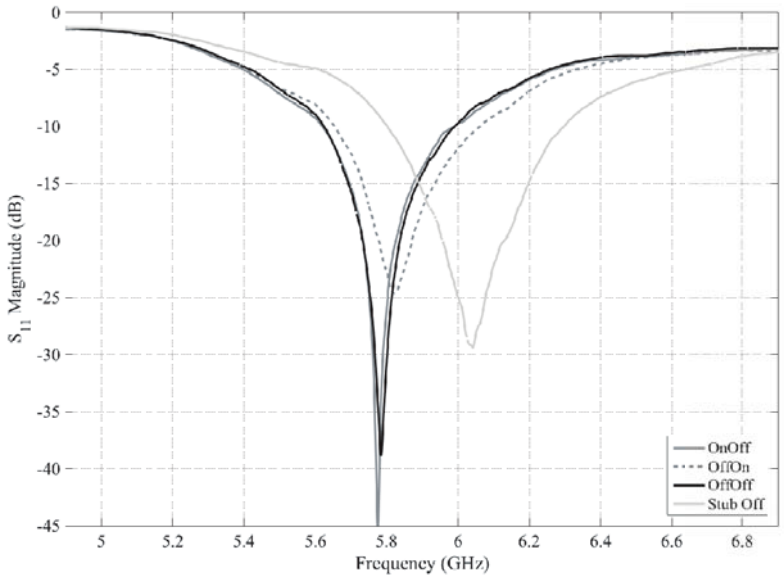

Figure 11. Measured reflection coefficient (S_{11}) of the printed ESPAR antenna mounted inside the shark-fin.

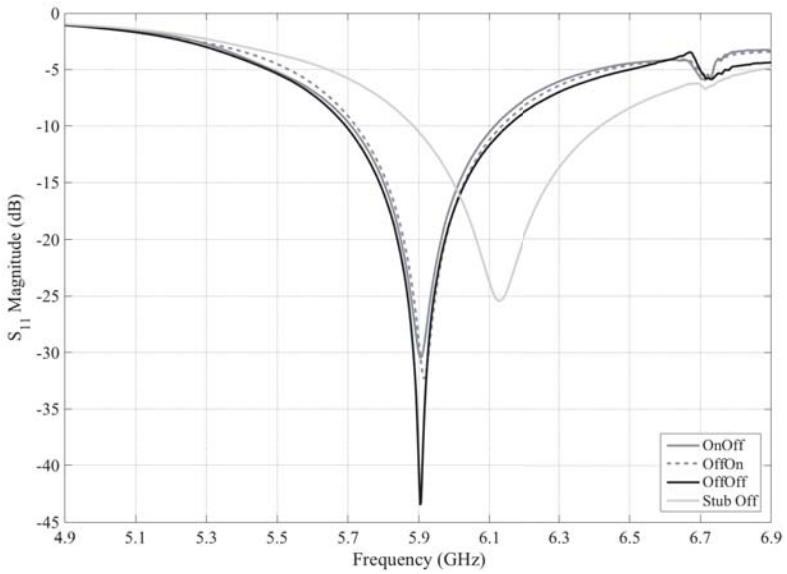

Figure 12. Simulated reflection coefficient (S_{11}) of the modified printed ESPAR antenna mounted inside the shark-fin.

The final measurement scenario involves the shark-fin antenna mounted on a 50×50 cm rectangular ground plane (GP). As can be observed in Fig. 16, a realised gain of 4 dB is observed in the OFF-ON state, while at the OFF-OFF state the gain value is 1 dB, meaning a gain improvement of 3 dB. In the ON-OFF state, there is a 5 dB increase (5.3 instead of 0.3 dB) that is attributed again to the shark-fin effect.

The elevation pattern (Fig. 17) shows a symmetrical behavior at the OFF-OFF state with θ at $\pm 90^\circ$ being at 0 dB absolute gain level, showing no deterioration from the free space and shark-fin integrated antenna cases. However, there is an unavoidable maximum gain tilt due to the presence of the metallic surface. Specifically, the maximum gain at the OFF-ON state is 8 dB at $\theta = -53^\circ$ that means a tilt of 37° from the horizon, and at the ON-OFF state it is 10 dB at $\theta = -56^\circ$. These results

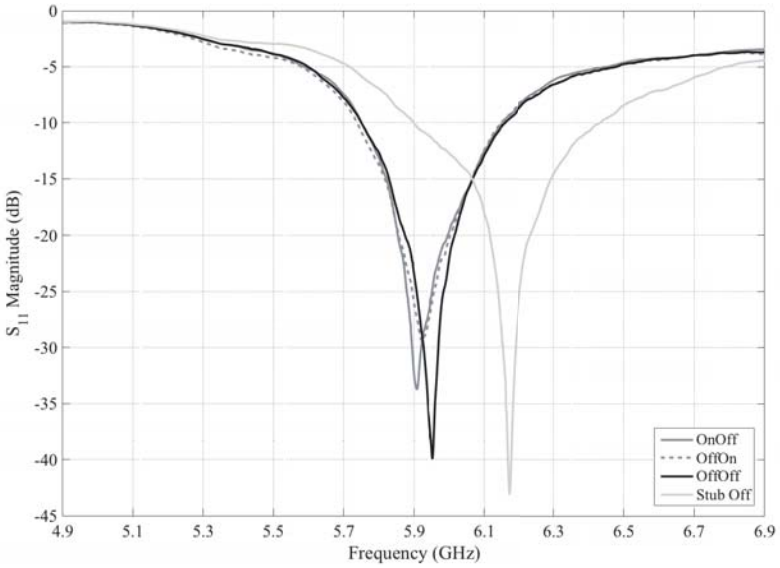

Figure 13. Measured reflection coefficient (S_{11}) of the modified printed ESPAR antenna mounted inside the shark-fin.

show the consistency in the antenna performance from the free space to the integrated performance on top of the GP. It is also evident that a null appears in the radiation patterns at the E-plane. It is fixed at 25° above the horizontal plane ($\theta = 90°$). This null is independent of the GP size and is attributed to the blind angle created by the contribution of a monopole due to image theory. In addition, the effect of the shark-fin casing to the resulted beam width of the directive states through measurements is investigated. Only the azimuth plane is considered in this study.

In the OFF-ON state, where the maximum gain is directed towards the backside of the shark-fin ($\varphi = 0°$), the beamwidth value remains almost unaffected, with 85° in free space, 79° inside the shark-fin, and 85° on top of the GP. On the contrary, at the ON-OFF state, where the maximum gain is directed towards the front part of the shark-fin ($\varphi = 180°$), the beamwidth is reduced, starting from 118° in free space, 83° inside the shark-fin, to 68° on top of the GP. Finally, as far as the antenna efficiency is concerned, it is found through simulations that it is not affected from the antenna integration inside the shark-fin (and over a 50×50 cm ground plane) since it remains above 94% at all the antenna operating states (Fig. 18).

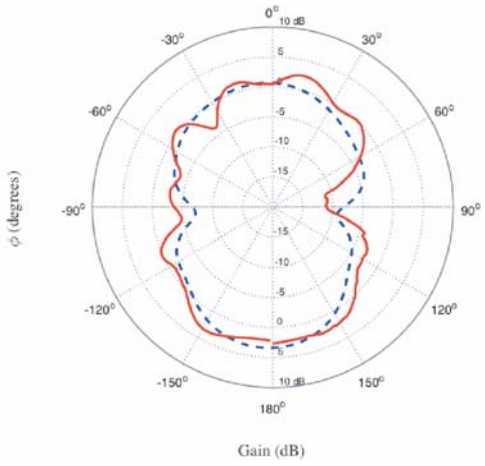

(a)

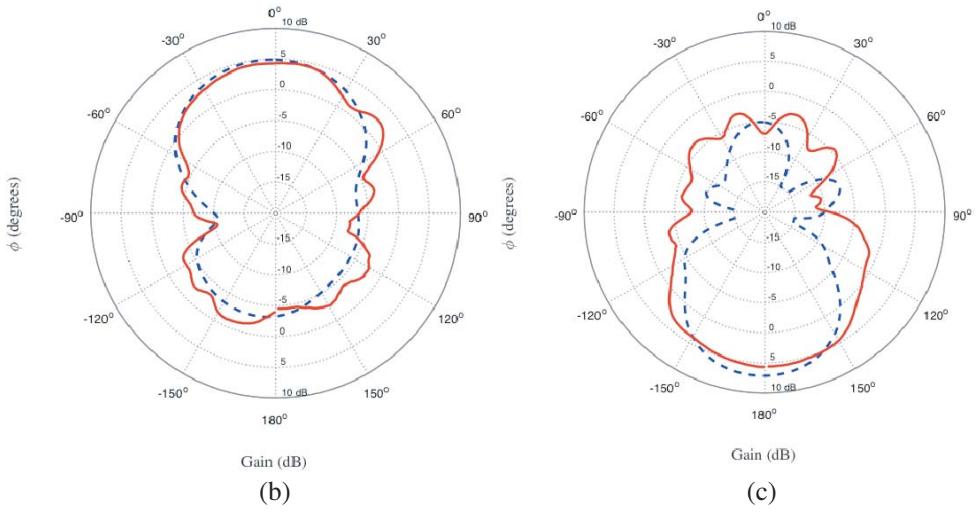

Figure 14. Measured (solid line) and simulated (dashed line) radiation patterns of the realised gain in the H-plane ($\varphi = 180°$) for the (a) OFF-OFF, (b) OFF-ON and (c) ON-OFF state of the ESPAR antenna inside the shark-fin.

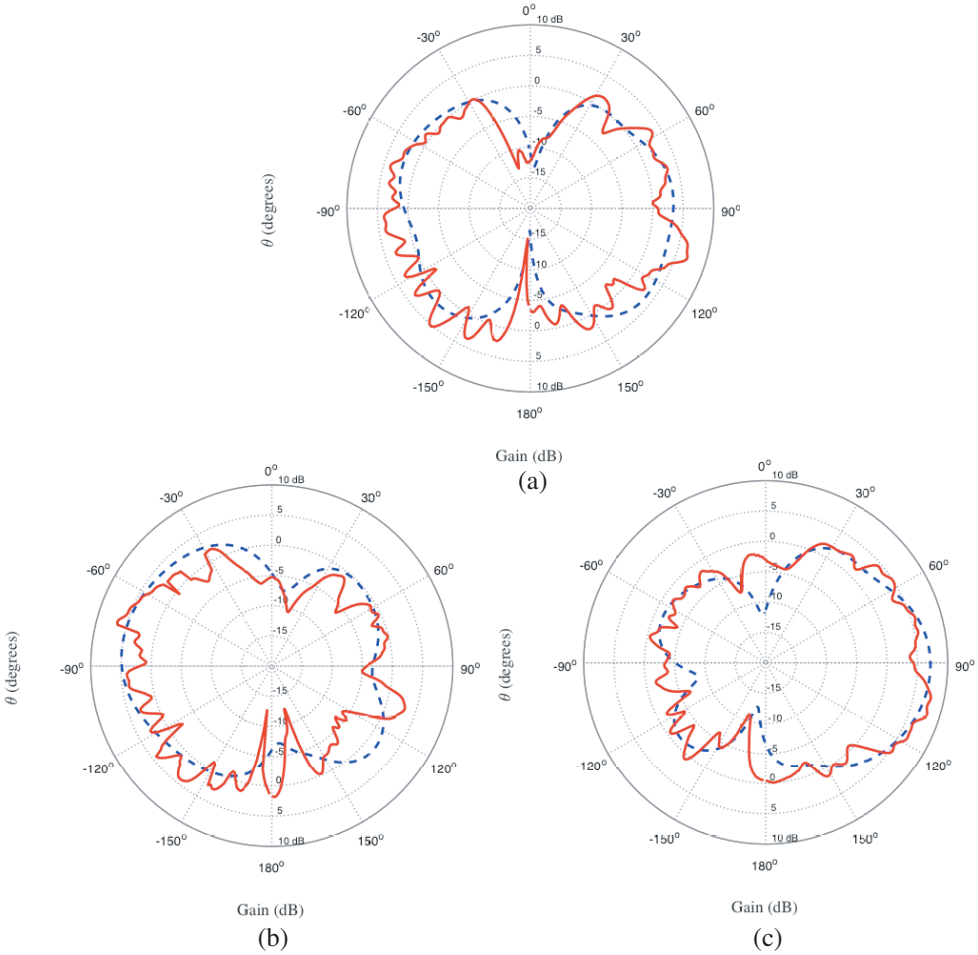

Figure 15. Measured (solid line) and simulated (dashed line) radiation patterns of the realised gain in the E-plane ($\theta = 90°$) for the (a) OFF-OFF, (b) OFF-ON and (c) ON-OFF state of the ESPAR antenna inside the shark-fin.

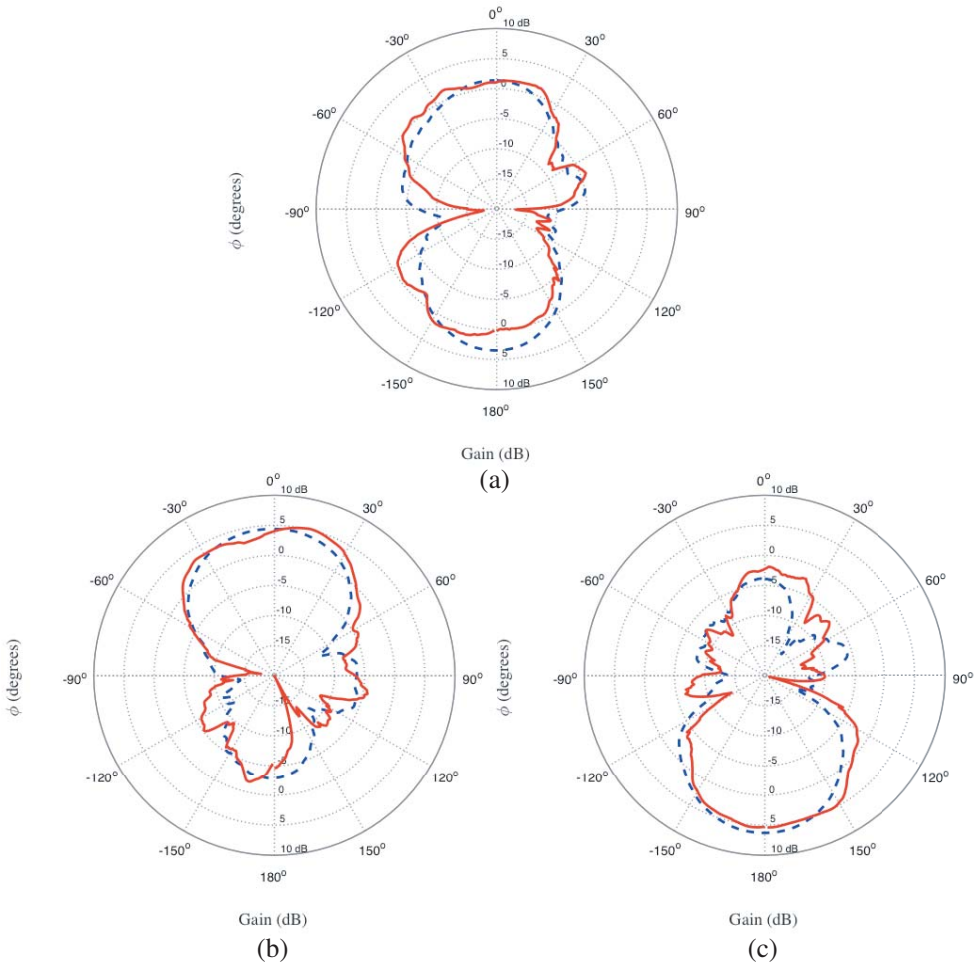

Figure 16. Measured (solid line) and simulated (dashed line) radiation patterns of the realised gain in the H-plane ($\varphi = 180°$) for the (a) OFF-OFF state, (b) OFF-ON and (c) ON-OFF state of the ESPAR antenna inside the shark-fin on top of the ground plane.

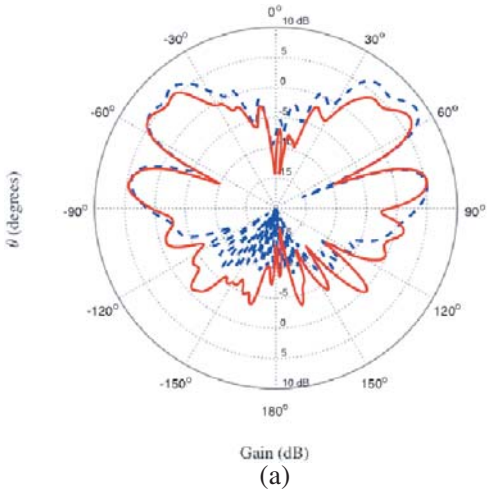

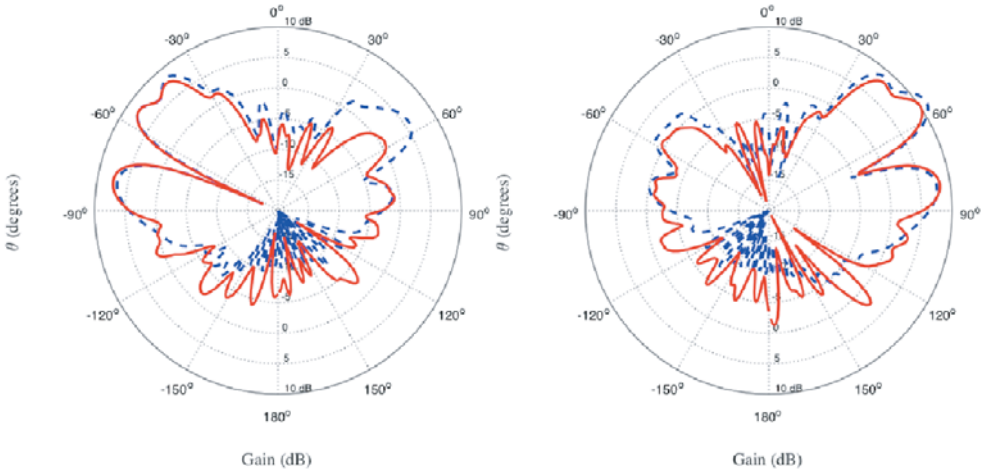

Figure 17. Measured (solid line) and simulated (dashed line) radiation patterns of the realised gain in the E-plane ($\theta = 90°$) for the (a) OFF-OFF state, (b) OFF-ON state and (c) ON-OFF state of the ESPAR antenna inside the sharkfin on top of the ground plane.

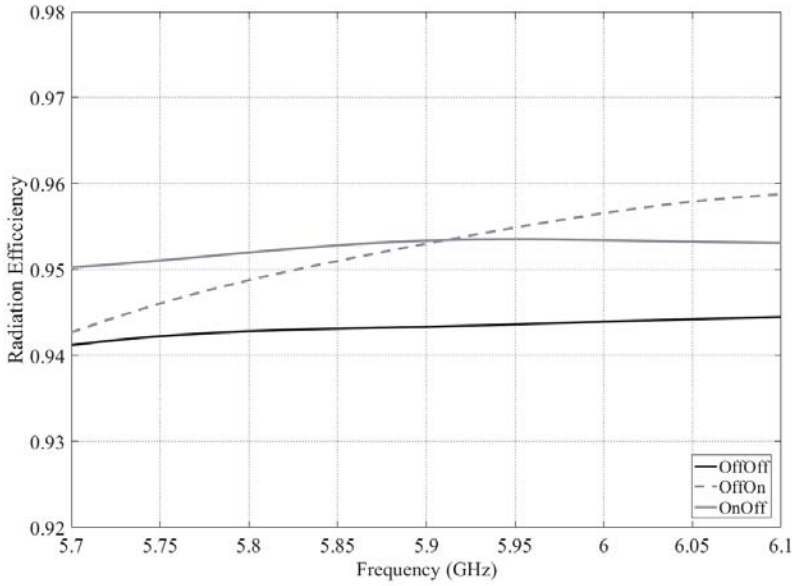

Figure 18. Radiation efficiency of the ESPAR antenna for all the operating states inside the shark-fin over a 50×50 cm ground plane.

4. CONCLUSION

In this paper, the design, development, and experimental verification of a novel V2X parasitic antenna array are thoroughly presented. The proposed ESPAR antenna demonstrates pattern reconfigurability (with one quasi-omni and two directive patterns), low cost, and compact size. The antenna system is designed to fit inside a shark-fin case mounted on the roof of a vehicle. A switched impedance matching network is embedded in the ESPAR design in order to enforce impedance matching for all states. The measured results demonstrate that the proposed antenna exhibits a performance in terms of return loss, radiation pattern, and reconfigurability which is suitable for the 5.9 GHz ITS V2X band.

ACKNOWLEDGMENT

This research is co-financed by Greece and the European Union (European Social Fund-ESF) through the Operational Programme Human Resources Development, Education and Lifelong Learning 2014–2020 in the context of the project "REPAIR (REconfigurable Parasitic Array for Intelligent TRansportation) (MIS 5007635)".

REFERENCES

1. Hobert, L., A. Festag, I. Llatser, L. Altomare, F. Visintainer, and A. Kovacs, "Enhancements of V2X communication in support of cooperative autonomous driving," *IEEE Communications Magazine*, Vol. 53, No. 12, 64–70, 2015.
2. Öncü, S., N. van de Wouw, W. M. H. Heemels, and H. Nijmeijer, "String stability of interconnected vehicles under communication constraints," *2012 IEEE 51st IEEE Conference on Decision and Control (CDC)*, 2459–2464, 2012.
3. Molisch, A. F., F. Tufvesson, J. Karedal, and C. F. Mecklenbrauker, "A survey on vehicle-to-vehicle propagation channels," *IEEE Wireless Communications*, Vol. 16, No. 6, 12–22, 2009.
4. Geissler, M., K. Scharwies, and J. Christ, "Intelligent antenna systems for cars," *GeMiC 2014; German Microwave Conference*, 1–3, VDE, 2014.
5. Rabinovich, V. and N. Alexandrov, "Compact car-mounted arrays," *Antenna Arrays and Automotive Applications*, 1–20, Springer, 2013.
6. Thiel, A., O. Klemp, A. Paiera, L. Bernadó, J. Karedal, and A. Kwoczek, "In-situ vehicular antenna integration and design aspects for vehicle-to-vehicle communications," *Proceedings of the Fourth European Conference on Antennas and Propagation*, 1–5, IEEE, 2010.
7. Liu, F., Z. Zhang, W. Chen, Z. Feng, and M. F. Iskander, "An endfire beam-switchable antenna array used in vehicular environment," *IEEE Antennas and Wireless Propagation Letters*, Vol. 9, 195–198, 2010.
8. Schack, M., D. Kornek, E. Slottke, and T. Kurner, "Analysis of channel parameters for different antenna configurations in vehicular environments," *2010 IEEE 72nd Vehicular Technology Conference-Fall*, 1–5, 2010.
9. Guan, N., H. Tayama, M. Ueyama, Y. Yoshijima, and H. Chiba, "A roof automobile module for LTE-MIMO antennas," *2015 IEEE-APS Topical Conference on Antennas and Propagation in Wireless Communications (APWC)*, 387–391, 2015.
10. Li, X.-L., G.-M. Yang, and Y.-Q. Jin, "Isolation enhancement of wideband vehicular antenna array using fractal decoupling structure," *IEEE Antennas and Wireless Propagation Letters*, Vol. 18, No. 9, 1799–1803, 2019.
11. Thiel, A., L. Ekiz, O. Klemp, and M. Schultz, "Automotive grade MIMO antenna setup and performance evaluation for LTE-communications," *2013 International Workshop on Antenna Technology (iWAT)*, 171–174, IEEE, 2013.
12. Bai, D., S. S. Ghassemzadeh, R. R. Miller, and V. Tarokh, "Beam selection gain versus antenna selection gain," *IEEE Transactions on Information Theory*, Vol. 57, No. 10, 6603–6618, 2011.
13. Marantis, L., K. Maliatsos, C. Oikonomopoulos-Zachos, D. K. Rongas, A. Paraskevopoulos, A. Aspreas, and A. G. Kanatas, "The pattern selection capability of a printed ESPAR antenna," *2017 11th European Conference on Antennas and Propagation (EUCAP)*, 922–926, IEEE, 2017.
14. Kim, S., D. Kang, and J. Choi, "Beam reconfigurable antenna using switchable parasitic elements for V2V applications," *2017 International Symposium on Antennas and Propagation (ISAP)*, 1–2, IEEE, 2017.
15. Kowalewski, J., J. Mayer, T. Mahler, and T. Zwick, "A compact pattern reconfigurable antenna utilizing multiple monopoles," *2016 International Workshop on Antenna Technology (iWAT)*, 1–4, IEEE, 2016.

16. Kowalewski, J., T. Mahler, J. Mayer, and T. Zwick, "A miniaturized pattern reconfigurable antenna for automotive applications," *2016 10th European Conference on Antennas and Propagation (EuCAP)*, 1–4, IEEE, 2016.
17. Harrington, R., "Reactively controlled directive arrays," *IEEE Transactions on Antennas and Propagation*, Vol. 26, No. 3, 390–395, 1978.
18. Kalis, A., A. G. Kanatas, and C. B. Papadias, "A novel approach to MIMO transmission using a single RF front end," *IEEE Journal on Selected Areas in Communications*, Vol. 26, No. 6, 972–980, 2008.
19. Ohira, T. and K. Gyoda, "Electronically steerable passive array radiator antennas for low-cost analog adaptive beamforming," *Proceedings 2000 IEEE International Conference on Phased Array Systems and Technology (Cat. No. 00TH8510)*, 101–104, IEEE, 2000.
20. Thiel, D. V. and S. Smith, *Switched Parasitic Antennas for Cellular Communications*, Artech House, 2002.
21. Kalis, A., A. G. Kanatas, and C. B. Papadias, *Parasitic Antenna Arrays for Wireless MIMO Systems*, Springer, 2014.
22. Anbaran, A. G., A. Mohammadi, and A. Abdipour, "Capacity enhancement of ad hoc networks using a new single-RF compact beamforming scheme," *IEEE Transactions on Antennas and Propagation*, Vol. 63, No. 11, 5026–5034, 2015.
23. Liu, H.-T., S. Gao, and T.-H. Loh, "Electrically small and low cost smart antenna for wireless communication," *IEEE Transactions on Antennas and Propagation*, Vol. 60, No. 3, 1540–1549, 2011.
24. Alrabadi, O. N., J. Perruisseau-Carrier, and A. Kalis, "MIMO transmission using a single RF source: Theory and antenna design," *IEEE Transactions on Antennas and Propagation*, Vol. 60, No. 2, 654–664, 2011.
25. Zhang, S., G. Huff, J. Feng, and J. T. Bernhard, "A pattern reconfigurable microstrip parasitic array," *IEEE Transactions on Antennas and Propagation*, Vol. 52, No. 10, 2773–2776, 2004.
26. Petit, L., L. Dussopt, and J.-M. Laheurte, "MEMS-switched parasitic-antenna array for radiation pattern diversity," *IEEE Transactions on Antennas and Propagation*, Vol. 54, No. 9, 2624–2631, 2006.
27. Preston, S., D. Thiel, J. W. Lu, S. O'Keefe, and T. Bird, "Electronic beam steering using switched parasitic patch elements," *Electronics Letters*, Vol. 33, No. 1, 7–8, 1997.
28. Islam, M. R. and M. Ali, "Elevation plane beam scanning of a novel parasitic array radiator antenna for 1900 MHz mobile handheld terminals," *IEEE Transactions on Antennas and Propagation*, Vol. 58, No. 10, 3344–3352, 2010.
29. Yousefbeiki, M. and J. Perruisseau-Carrier, "Towards compact and frequency-tunable antenna solutions for MIMO transmission with a single RF chain," *IEEE Transactions on Antennas and Propagation*, Vol. 62, No. 3, 1065–1073, 2013.
30. Sawaya, T., K. Iigusa, M. Taromaru, and T. Ohira, "Reactance diversity: proof-of-concept experiments in an indoor multipath-fading environment with a 5-GHz prototype planar ESPAR antenna," *First IEEE Consumer Communications and Networking Conference, CCNC 2004*, 678–680, IEEE, 2004.
31. Paraskevopoulos, A., D. Rongas, L. Marantis, and A. Kanatas, "Beam-switched ESPAR antenna with embedded matching network for V2X communications," *2019 PhotonIcs & Electromagnetics Research Symposium — Spring (PIERS — SPRING)*, 3619–3625, Rome, Italy, June 17–20, 2019.
32. Marantis, L., D. Rongas, A. Paraskevopoulos, C. Oikonomopoulos-Zachos, and A. Kanatas, "Pattern reconfigurable ESPAR antenna for vehicle-to-vehicle communications," *IET Microwaves, Antennas & Propagation*, Vol. 12, No. 3, 280–286, 2017.
33. Dassault Systemes, D. C., "CST Studio Suite 3D EM simulation and analysis software," https://www.3ds.com/products-services/simulia/products/cst-studio-suite, [Online].
34. GmbH, I., "Antenna measurements," 2019, http://www.imst.com/imst/en/development/antennas/measurements-test.php, [Online].